Electrorotation Studies of Baby Hamster Kidney Fibroblasts Infected with Herpes Simplex Virus Type 1

Steffen Archer,* Hywel Morgan,* and Frazer J. Rixon#
*Bioelectronics Research Centre, University of Glasgow, Glasgow G12 8QQ, and #Medical Research Council, Virology Unit, Glasgow G11 5JR, United Kingdom

ABSTRACT The dielectric properties of baby hamster kidney fibroblast (BHK(C-13)) cells have been measured using electrorotation before and after infection with herpes simplex virus type 1 (HSV-1). The dielectric properties and morphology of the cells were investigated as a function of time after infection. The mean specific capacitance of the uninfected cells was 2.0 μF/cm^2, reducing to a value of 1.5 μF/cm^2 at 12 h after infection. This change was interpreted as arising from changes in the cell membrane morphology coupled with alterations in the composition of the cell membrane as infection progressed. The measured changes in the cell capacitance were correlated with alterations in cellular morphology determined from scanning electron microscope (SEM) images. Between 9 and 12 h after infection the internal permittivity of the cell exhibited a rapid change, reducing in value from 75ϵ_o to 58ϵ_o, which can be correlated with the generation of large numbers of Golgi-derived membrane vesicles and enveloped viral capsids. The data are discussed in relation to the known life cycle of HSV-1 and indicate that electrorotation can be used to observe dynamic changes in both the dielectric and morphological properties of virus-infected cells. Calculations of the dielectrophoretic spectrum of uninfected and infected cells have been performed, and the results show that cells in the two states could be separated using appropriate frequencies and electrode arrays.

INTRODUCTION

Infection of cells by viruses frequently results in extensive alterations in the biochemistry and physiology of the cells. Although much effort has been expended on studying changes in gene expression after infection and the biochemical signals that control these changes, much less is known about the effect of infection on the physical properties of the cell. Consequently, we have used electrorotation methods to measure the dielectric properties of baby hamster kidney fibroblast cells (BHK(C-13)) after infection with herpes simplex virus type 1 (HSV-1). Recent developments in analyzing cells in rotating electric fields has demonstrated the value of this technique for analyzing the properties of single cells and determining their biophysical properties.

The infectious cycle of the virus can be summarized as follows. Upon infection, the virus envelope fuses with the cell's plasma membrane, releasing the capsid into the cytoplasm. The capsid is transported along the microtubule network (Sodeik et al., 1997) to the vicinity of a nuclear pore where the viral DNA is released and enters the nucleus. Viral gene expression and DNA replication ensue and progeny viral genomes are packaged into newly assembled capsids within the nucleus. The DNA-containing capsids leave the nucleus by budding through the inner nuclear membrane. Mature enveloped virions are then transported to the plasma membrane in Golgi-derived transport vesicles and are released onto the cell surface by exocytosis without cell lysis (Steven and Spear, 1997; Smith and Harven, 1973; Morgan et al., 1959; Johnson and Spear, 1982). In this paper we have analyzed this life cycle in terms of the time-dependent changes in the dielectric properties of single cells.

The dielectric properties of a cell (capacitance and conductance) reflect the composition and shape of the plasma membrane and also of the cell cytoplasm and nucleus. Any modifications induced by, for example, virus invasion will lead to changes in these dielectric properties. A common consequence of virus infection in animal cells is disruption of the cytoskeleton. This can lead to large-scale changes in cell conformation that are detectable through their effects on the electrorotational behavior.

The technique of electrorotation has been used to study the dielectric properties of a number of biological particles (Fuhr et al., 1985a,b; Wicher et al., 1987; Gimsa et al., 1989, 1991, 1994, 1996; Becker et al., 1995; Huang et al., 1995, 1996; Wang et al., 1997; Arnold and Zimmermann, 1988; Zhou et al., 1996; Arnold et al., 1989; Gascoyne et al., 1997; Hu et al., 1990). The method relies on observing the rotation of single particles exposed to a rotating electric field that is generated using suitable electrode structures (Arnold and Zimmermann, 1988). There are a number of examples where electrorotation has been used as a noninvasive method to probe the changes in the dielectric properties of cells and microorganisms when subjected to stimuli or challenged by infection or parasitic invasion.

Early electrorotation measurements of the time-dependent interaction of erythrocytes with influenza virus showed

Received for publication 10 August 1998 and in final form 21 December 1998.

Address reprint requests to Dr. Hywel Morgan, Department of Electronic and Electrical Engineering, University of Glasgow, Glasgow G23 8QQ, UK. Tel.: 44-141-330-5237; Fax: 44-141-330-4907; E-mail: h.morgan@elec.gla.ac.uk.

0006-3495/99/05/2833/10 $2.00

that changes in ion permeability could be followed using the technique (Gimsa et al., 1989). Electrorotation has also been used to study the effect of the biocide polyhexamide on the properties of yeast cells (Zhou et al., 1996) where the plasma membrane conductivity was observed to increase gradually with increasing biocide concentration. Differences in the membranes of fertilized and unfertilized rabbit oocytes (Arnold et al., 1989) have been observed, and the effects of antibiotics on the membranes of human erythrocytes (Gimsa et al., 1994) have also been followed. In this case the effect of the antibiotic nystatin was to induce a rapid increase in transmembrane permeability coupled with shrinkage of the cells, both of which could be determined through their influence on electrorotation properties. Recent work has shown that infection of erythrocytes with the malaria parasite *Plasmodium falciparum* causes a time-dependent change in the rotation spectrum that is indicative of an outflux of ions via the plasma membrane (Gascoyne et al., 1997) consistent with the production of parasite-associated membrane pores.

Changes in the dielectric properties of lymphocytes after stimulation with mitotic agents were studied by Hu et al. (1990). Both B and T lymphocytes were challenged with mitotic agents, and the changes in the conductivity, permittivity, and morphology of the cells were followed as a function of time. The response was shown to parallel increases in transmembrane transport after mitogenic stimulation. Observations of the electrorotation properties of normal and malignant cells have shown that significant changes occur in the morphology and dielectric properties of cells during and after transformation (Huang et al., 1996). Recent advances in circuit design have enabled measurements to be made at frequencies up to 1.6 GHz (Gimsa et al., 1996; Holzel, 1997), allowing detailed dielectric data on the cell interior to be obtained. In particular, the dielectric relaxation of hemoglobin inside erythrocytes has been measured using high-frequency electrorotation techniques (Gimsa et al., 1996).

The technique of electrorotation allows measurements to be made of single cells within a mixture so that the dielectric properties of different subpopulations can be measured. These data can then be used to optimize conditions for cell sorting by dielectrophoretic methods (Becker et al., 1995; Stephens et al., 1996). In a similar vein, cells that have been infected with virus could also potentially be separated from uninfected cells using dielectrophoretic methods.

In this paper the electrorotation spectra of BHK(C-13) cells were measured up to 20 MHz, and the dielectric parameters of the membrane and cytoplasm obtained by fitting the data to a single-shell model that neglects the influence of the nucleus (Huang et al., 1992). The electrorotation data were interpreted in the light of known changes to the morphology and composition of the cells that follow virus infection and that can be observed by scanning electron microscopy (SEM) and examination of protein profiles.

MATERIALS AND METHODS

Cell culture and virus infection.

Cells from a tissue-culture-adapted baby hamster fibroblast (BHK21 C13) cell line were maintained in Glasgow-modified Eagle's medium (GIBCO/BRL) supplemented with 10% tryptose phosphate broth and 10% newborn calf serum. Cells were grown on 60-mm tissue culture plates (CORNING/UK), to a density of 5×10^6 cells/plate. These cells are normally adherent, and to obtain electrorotation spectra they were carefully removed from the culture dishes using mechanical methods.

To ensure simultaneous infection of all cells, 10 plaque-forming units (pfu) per cell of Ficol gradient purified HSV-1 strain 17 (Szilagyi and Cunningham, 1991) were used. The purified virus was stored at -70°C in aliquots of 50 μl. For each experiment a fresh aliquot was used. At appropriate times after infection the cells were harvested by scraping into the tissue culture medium, pelleted by centrifugation at $400 \times g$, and resuspended in the suspension medium used for electrorotation measurements, which consisted of 320 mM sucrose, 0.2 mM EDTA, 0.1 mM phosphate-buffered saline (PBS), and 0.3 mM polyethylene glycol.

Electrorotation measurements

When a particle such as a cell, suspended in an aqueous medium, is exposed to an electric field, it polarizes, giving rise to an induced dipole moment. For the case of a rotating electric field, there will be a phase difference between the field vector and the polarization vector so that the particle will experience a torque tending to align the particle's polarization vector with the field. This torque is zero when the phase angle between the particle's polarization vector and the applied field is zero and maximal when the phase angle is $\pm 90°$. If the induced dipole moment lags behind the field, then the direction of rotation is with the field and vice versa for a moment that leads the field. A theoretical treatment of this effect can be found in a number of publications (Gimsa et al., 1996; Huang et al., 1992; Pethig, 1991; Wang et al., 1992, 1993).

The rotating electric field was generated from a four-phase direct digital synthesized frequency generator, designed and constructed in-house. Four-electrode polynomial arrays were used for the measurements (Holzel, 1993; Huang and Pethig, 1991), with the distance between opposing tips of 800 μm. The electrodes were fabricated by evaporating a layered structure of gold/palladium/titanium onto glass microscope slides using standard photolithographic techniques (Green, 1998).

Electrorotational measurements were obtained from BHK(C-13) cells that had been harvested and resuspended at a concentration of approximately 10^4 cells per ml in a suspending medium with a conductivity of 17.5 mSm^{-1}, at a temperature of 20°C. The conductivity of the medium was measured using a Hewlett-Packard 4192A impedance analyzer with a Sentek conductivity cell at a frequency of 100 kHz. For the electrorotation measurements, a chamber was constructed around the electrode array with a volume of approximately 1 ml and sealed with a coverslip. The entire electrode chamber assembly was placed on an inverted microscope, and cell rotation was imaged with a CCD camera and recorded using S-VHS video. The frequency-dependent rotation rate was measured using a stopwatch. The spectrum of single isolated cells, which were located within the central area of the electrode array (Hughes et al., 1994), were measured at four points per decade over the frequency range 3 kHz to 20 MHz at a voltage of 2 V (rms) connected to the four electrodes in phase quadrature.

SEM images

At appropriate times after infection, the culture medium was removed from the culture dish and the cell monolayer was carefully washed with PBS. The cells were then scraped into fresh PBS and allowed to settle onto glass coverslips coated with poly-L-lysine. After 5 min, unattached cells were removed by rinsing in fresh PBS. Adsorbed cells were fixed with a 2.5% solution of glutaraldehyde in PBS for 1 h, rinsed in PBS, and exposed to 1% osmium tetroxide for another hour. The cells were dehydrated by

sequential immersion in 30%, 50%, 70%, 90%, and 2X 100% ethanol followed by a 50:50 ethanol:acetone solution and then 100% acetone. Cells were then sputter coated with gold. Images were taken at a magnification of 5×10^3 on a HITACHI-S800 SEM operating at 30 kV.

Protein profiles

The cells for protein analysis were harvested at the same times after infection as cells used for electrorotation and SEM analysis. For protein radiolabeling experiments, cells were infected in Glasgow-modified Eagle's medium containing 2% newborn calf serum and one-fifth the normal concentration of methionine. Three hours after infection, 50 mCi/ml of [^{35}S]methionine was added and incubation was continued until the appropriate time after infection for harvesting. Samples were prepared for electrophoresis, and proteins were separated on polyacrylamide gels as described elsewhere (Leslie et al., 1996). Gels were fixed, dried, and exposed for autoradiography using Kodak X-O-mat S film.

Data analysis and theory

When in suspension, BHK cells are spherical in shape so they can be approximated to a series of concentric spheres, consisting of the plasma membrane, the cytoplasm, the nuclear membrane, and the nucleus. Owing to the limited-frequency bandwidth of our experimental apparatus, it was not possible to obtain data at sufficiently high frequencies to probe the nucleus and the nuclear membrane. Thus, the cells were modeled using a single-shell model, which considers only the membrane and the cytoplasm, the nucleus being considered as part of the cytoplasm. Analysis of the data in terms of this simple model has been found to be remarkably effective and gives reproducible values for the conductivity and permittivity of the membrane and of the interior of the cell (Wang et al., 1994). The specific membrane capacitance is calculated in terms of the membrane permittivity according to $C_{spec} + \epsilon_{mem}/d$, where d is the membrane thickness and ϵ_{mem} is the permittivity of the membrane.

The steady-state rotation rate $R(\omega)$ depends upon the frequency of the electric field (Arnold and Zimmermann, 1988) according to the following expression:

$$R(\omega) = -\frac{\epsilon_{med}\mathrm{Im}\left(\frac{\epsilon_p^* - \epsilon_{med}^*}{\epsilon_p^* + 2\epsilon_{med}^*}\right)E^2}{2\eta}K, \quad (1)$$

where K is a scaling factor that is introduced to take into account that neither the viscosity (η) nor the electric field strength (E) are precisely known. ϵ_{med} is the real component of the permittivity of the suspension medium, ϵ_{med}^* and ϵ_p^* are the complex permittivities of the suspending medium and the particle, respectively, and a general complex permittivity is given by $\epsilon^* = \epsilon - j(\sigma/\omega)$, where σ is the conductivity. According to the smeared-out-shell model, the complex permittivity of the particle can be written as the sum of the membrane and internal complex permittivities (Wang et al., 1994):

$$\epsilon_p^* = \frac{\left[\frac{r}{r-d}\right]^3 + 2\left[\frac{\epsilon_{int}^* - \epsilon_{mem}^*}{\epsilon_{int}^* + 2\epsilon_{mem}^*}\right]}{\left[\frac{r}{r-d}\right]^3 - \left[\frac{\epsilon_{int}^* - \epsilon_{mem}^*}{\epsilon_{int}^* + 2\epsilon_{mem}^*}\right]}, \quad (2)$$

where r is the radius of the cell and ϵ_{int}^* and ϵ_{mem}^* are the complex permittivities of the cell interior and membrane, respectively. Using curve-fitting procedures the dielectric parameters of the cells can thus be obtained.

The dielectric parameters of the cells were obtained from Eqs. 1 and 2 using an algorithm that minimizes the sum of the deviations between the experimental rotation spectrum ($R_{expt}(\omega_i)$) and the spectrum predicted by the single-shell model of a cell with a steady-state rotation rate ($R_{est}(\omega_i)$) (Gascoyne et al., 1995). For i data points this function can be written as:

$$\mathrm{Min}\left[\sum_i (R_{expt}(\omega_i) - R_{est}(\omega_i))^2\right]. \quad (3)$$

Curve fitting was carried out using a nonlinear Nelder-Mead simplex method using Matlab software. Using this procedure, the specific membrane capacitance (C_{spec}), the internal permittivity (ϵ_{int}), and the internal conductivity (σ_{int}) of the cell were obtained. The membrane conductivity of the cells was extremely low and impossible to accurately predict from electrorotation data. To estimate the membrane conductivity, dielectrophoretic crossover frequency methods were used as outlined in Huang et al., 1996. Using this technique, the membrane conductivity of 30 different cells, both before and after infection, was measured. In all cases, the membrane conductivity was found to be too low to accurately measure, so for the purpose of fitting the electrorotation data the conductivity of the membrane was set to a fixed value of $\sigma_{mem} = 5 \times 10^{-7}$ Sm^{-1}.

To quantify the accuracy of curve fitting, a regression coefficient (ρ) was calculated according to:

$$\rho = 1 - \left[\frac{\sum_i (R_{expt}(\omega_i) - R_{est}(\omega_i))^2}{\sum_i (R_{expt}(\omega_i))^2}\right]. \quad (4)$$

A value close to unity for the regression coefficient implies that the model used to fit the electrorotational data was successful. Only data in which the regression coefficient was greater than 0.985 were used. Data sets that produced a regression coefficient less than this value were rejected.

RESULTS

Electrorotation data

Electrorotational spectra for HSV-1-infected BHK(C-13) cells were obtained at discrete times throughout a single cycle of virus replication. The time points chosen were at 0, 6, 9, 12, 18, and 26 h after infection. At each time point, electrorotational spectra were obtained for 8 to 10 individual cells. To ensure the reproducibility of the results, the time courses were performed in two ways.

Method 1: discontinuous time course

In this approach, each time point (five data sets in total) was treated as a separate experiment. Thus, five culture dishes were infected simultaneously with 10 pfu of virus per cell. They were incubated at 37°C, and at the appropriate time after infection (e.g., 6 h), all of the cells were harvested. The cells were stored in growth medium at 4°C, and electrorotation spectra taken as soon as possible. As each spectrum took approximately 30 min, to accumulate up to 10 spectra (sequentially) took several hours. Typically, two to three spectra (each representing a single cell) were obtained from one plate of cells. Therefore, using this method, up to 10 electrorotational spectra were obtained for each time point.

Method 2: continuous time course

In method 1, above, all of the batches of cells being examined were harvested at the same time and stored at 4°C until used for measurement. Although metabolic processes are

greatly delayed at low temperatures, we felt it necessary to confirm that the behavior of the cells was not affected by this treatment. As an alternative approach, therefore, five replicate plates of cells were infected simultaneously with virus. The plates were incubated at 37°C, and at each of the desired times (e.g., 6 h) one was removed, the cells were harvested, and electrorotation spectra determined immediately. Incubation of the remaining plates was continued until the next time point when the process was repeated. At each time point, two to four spectra were collected. To obtain the required number of electrorotational spectra needed to determine average values for the cell properties at each time point, this entire procedure was repeated three times.

A rotation spectrum for an uninfected BHK(C-13) cell is shown in Fig. 1 *a*. This cell had been cultured to confluence before being physically removed from the culture dish surface and its spectrum recorded. At a medium conductivity of 17.5 mSm^{-1} the cell exhibits an anti-field rotation peak at approximately 30 kHz. The best fit to the data is shown by the solid line, and for this particular cell the parameter set used to obtain this fit is given by $C_{spec} = 2.30\ \mu F/cm^2$, $\sigma_{int} = 0.23\ Sm^{-1}$, and $\epsilon_{int} = 61\epsilon_o$ with $r = 6.7\ \mu m$. A typical electrorotation spectrum for a BHK cell 18 h after infection is shown in Fig. 1 *b*, and in this case a best fit was obtained with $C_{spec} = 1.52\ \mu F/cm^2$, $\sigma_{int} = 0.45\ Sm^{-1}$, and $\epsilon_{int} = 46\epsilon_o$ with $r = 6.8\ \mu m$. These data show that (for the same medium conductivity) the infected cell exhibits an anti-field rotation peak at approximately 50 kHz.

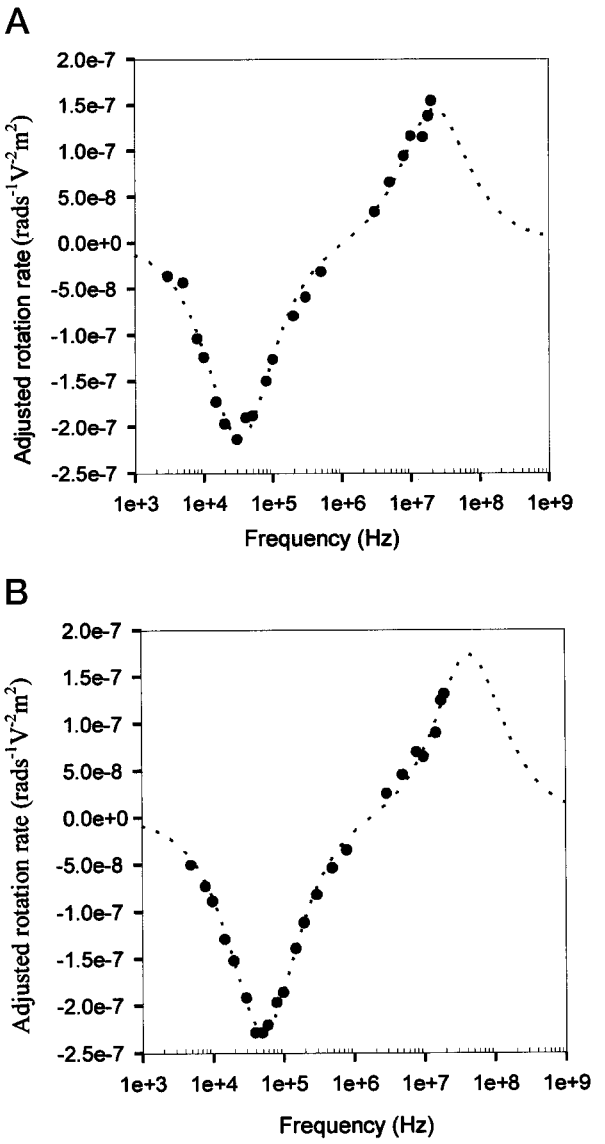

FIGURE 1 (*a*) Typical electrorotation spectra for an uninfected BHK(C-13) cell. The solid line represents the best fit to the experimental data. The best-fit dielectric parameters for this particular cell were $C_{spec} = 2.30\ \mu F/cm^2$, $\epsilon_{int} = 61\epsilon_0$, and $\sigma_{int} = 0.23\ Sm^{-1}$. The regression coefficient was $\rho = 0.994$. (*b*) Typical electrorotational spectrum for a BHK(C-13) cell, 18 h after infection with HSV-1 at 10 pfu. Solid line represents the best fit to the experimental data. The best-fit dielectric parameters derived for this particular cell were: $C_{spec} = 1.52\ \mu F/cm^2$, $\epsilon_{int} = 46\epsilon_0$, and $\sigma_{int} = 0.45\ Sm^{-1}$. The regression coefficient was $\rho = 0.996$.

Protein profiles

To confirm that the cells being analyzed in the electrorotation studies were properly infected, protein synthesis was analyzed by labeling the cells with [^{35}S]methionine. The protein profiles at times 0, 6, 9, 12, 18, and 26 h after infection are shown in Fig. 2, with several of the more prominent virus-specific proteins labeled. As expected, viral proteins, including structural components of the capsid (VP5), tegument (VP16 and VP22), and envelope (gB), are present in increasing amounts from 6 h after infection. The time course of protein synthesis is typical for HSV-1 infected BHK cells (Leslie et al., 1996) and demonstrates that the infection is progressing normally under these experimental conditions.

Specific membrane capacitance

The time-dependent changes in the specific membrane capacitance of BHK(C-13) cells after infection for both the interrupted and the continuous time courses are plotted in Fig. 3. The data plotted in this figure represent the mean of the specific membrane capacitances with standard errors also shown. The membrane thickness *d* was set at 7 nm to obtain these data.

It can be seen from Fig. 3 that a gradual decrease in the specific membrane capacitance of the cells occurs with time after infection with HSV-1. The same decrease is observed for both the interrupted and the continuous time course experiments. The capacitance of the uninfected cells is 2.0 $\mu F/cm^2$, which decreases to 1.6–1.8 $\mu F/cm^2$ 9 h after infection. There was a steady decrease with time up to 18 h after infection, when the capacitance reached 1.25 $\mu F/cm^2$. The specific membrane capacitance then increased again to a final value of 1.5 $\mu F/cm^2$ at 26 h after infection.

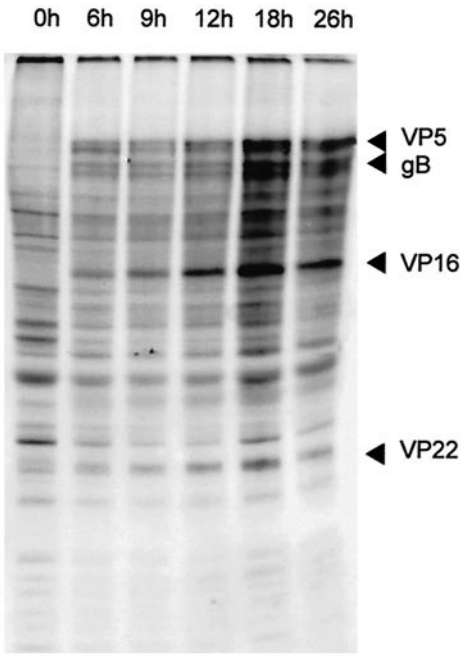

FIGURE 2 Protein profiles of HSV-1-infected BHK(C-13) cells. The figure shows the protein profiles for the cells at time 0, 6, 9, 12, 18, and 26 h after infection, and structural components of the capsid (VP5), tegument (VP16 and VP22), and envelope (gB) are present in increasing amounts from 6 h after infection.

Surface morphology and membrane composition

Implicit in the single-shell model is the assumption that the surface is smooth. However, as Fig. 4 shows, the surface of a real cell differs considerably from the ideal. The cell membrane is composed of a lipid bilayer, with a number of biomolecules, such as cholesterol and ion channels, spanning part of or the whole thickness of the membrane. In electrical terms, these different regions can be modeled as a number of separate electrical components in parallel so that the specific membrane capacitance can be described by the following simple expression (Wang et al., 1994):

$$C_{spec} = \alpha C_{lip} + (1 - \alpha) C_{other}, \quad (5)$$

where α is the fraction of the cell surface composed of lipid bilayer, and the subscripts lip and other refer to the lipid bilayer and other components (biomolecules), respectively.

It has been estimated for mammalian cells (Wang et al., 1994) that values for these membrane parameters are $C_{lip} = 0.78\ \mu F/cm^2$ and $C_{other} = 1.04\ \mu F/cm^2$. Assuming that typically 60% of the membrane surface consists of biomolecules other than the lipid bilayer (i.e., $\alpha = 0.4$), then $C_{spec} = 2.01\ \mu F/cm^2$, which is too low to account for the measured values for BHK(C-13) cells. The maximum C_{spec} allowed by the model is with $\alpha = 0$, i.e., $C_{spec} = 1.04\ \mu F/cm^2$, compared with values of $C_{spec} = 2.01\ \mu F/cm^2$ obtained for BHK cells. Thus, in general, this approach is inadequate to explain the specific membrane capacitance measured for the BHK(C-13) cells.

To account for such discrepancies, the concept of a folding factor ϕ_{mem} was proposed (Hu et al., 1990; Wang et al.,

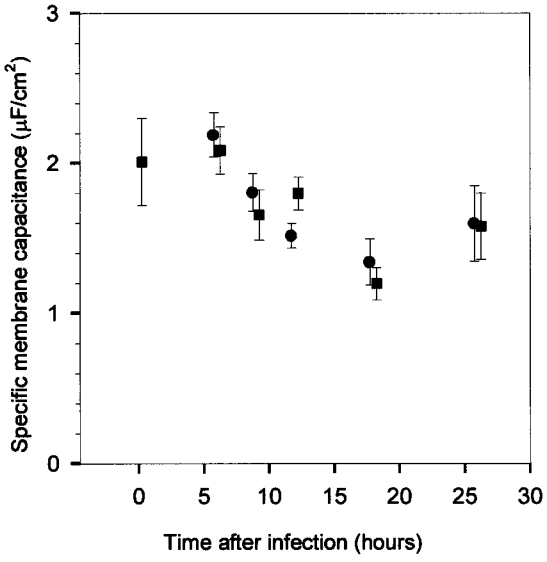

FIGURE 3 Plot of the change in the specific membrane capacitance of BHK(C-13) cells after infection with HSV-1. ●, continuous; ■, discontinuous time course experiments. For clarity, the points have been offset on the time axis by +0.25 h for the discontinuous and −0.25 h for the continuous time course. Vertical bars show the standard error.

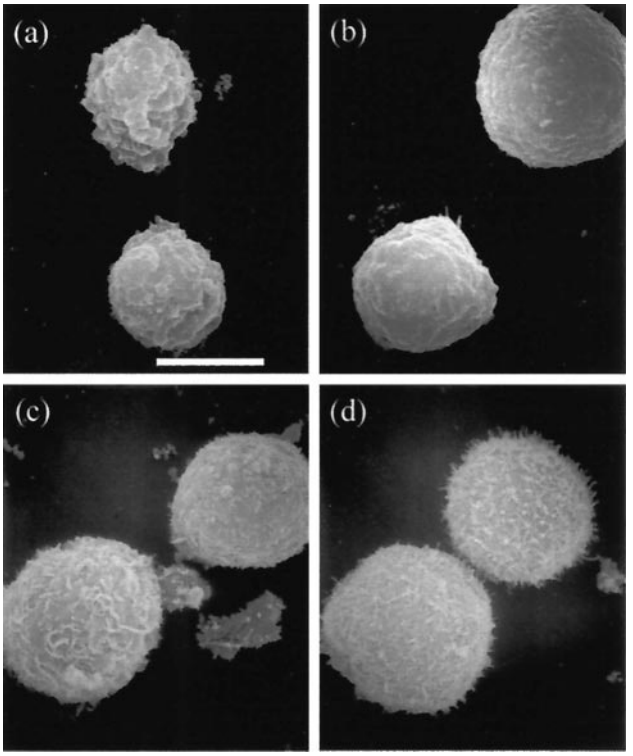

FIGURE 4 SEM photographs of BHK(C-13) at various stages of infection cycle. (*a*) Uninfected BHK(C-13) cell; remaining BHK(C-13) cells were infected with 10 pfu/cell for HSV-1 for 9 h (*b*), 18 h (*c*), and 26h (*d*). All cells were harvested and prepared for microscopy as described in Materials and Methods. Scale bar, 6 μm.

1994) to take into account that, due to features such as microvilli, folds, ruffles, and blebs, a cell surface is highly irregular and invaginated. The specific membrane capacitance can then be written as:

$$C_{spec} = \phi_{mem}[\alpha C_{lip} + (1 - \alpha)C_{other}]. \quad (6)$$

The membrane of a BHK cell contains a number of different proteins that span part of or the whole thickness of the membrane. Such a membrane would be expected to have a high membrane capacitance (as α would be low). The herpes virus particle contains 12 or more integral envelope proteins. As infection proceeds, these proteins are synthesized in increasing amounts, and most are inserted into cellular membranes, including the plasma membrane (Hutchinson et al., 1995). In parallel with this process, synthesis of many host cell proteins is inhibited. Consequently, as infection progresses, the composition of the cell membrane tends to approach that of the viral envelope. Viral glycoproteins are known to span the viral envelope, but as the virus is nonmetabolizing, there are no ion channels in its envelope. Thus, it is possible that the viral membrane may have a lower membrane capacitance than the BHK cell membrane. The reduction in the specific membrane capacitance of the plasma membrane throughout infection may therefore reflect the convergence of its properties toward those of the virus envelope.

Scanning electron microscopy

The time-dependent changes in the membrane folding factor after virus infection were observed by SEM. Examples of mock-infected cells and infected cells at times 9, 18, and 26 h after infection are shown in Fig. 4.

These images reveal that there are no dramatic changes to the overall appearance of the cells after infection. However, differences in their surface morphologies can be seen at the different times. Thus, in comparison with infected cells, uninfected cells (Fig. 4 *a*) are less uniformly spherical and have a surface membrane that has few microvilli but shows evidence of large-scale irregularities, such as folds and ruffles. Cells that have been infected for 9 h (Fig. 4 *b*) are rounder and have membranes that exhibit greater roughness, on a small scale, than in uninfected cells. There is an increase in the number of microvilli, and there seems to be a reduction in the large-scale features apparent in the uninfected cells. These changes are even more pronounced at 18 and 26 h after infection (Fig. 4, *c* and *d*), where the cell surface is uniformly rounded with an additional increase in the number of microvilli, as time progresses.

From the images shown in Fig. 4 there appear to be two factors that affect the cell folding factor throughout the life cycle of the virus. Mock-infected cells have a surface with large-scale folding but relatively little small-scale roughness due to microvilli. After infection, the shape of the cells becomes more uniform; the large-scale folding is lost and microvilli become increasingly evident. The reduction in the large-scale folding observed with time would be expected to reduce the membrane folding factor, whereas the presence of microvilli could cause a smaller increase. Another possible reason for the observed drop in the membrane capacitance is that the composition of the cell membrane changes during the infection cycle, tending toward the properties of the viral envelope.

A small increase in the specific membrane capacitance of the cells occurs at the end of the virus life cycle. This could be due to an additional increase in the number of microvilli on the cell surface, giving rise to an increase in the membrane folding factor at 26 h after infection.

Internal permittivity

The time-dependent changes in the internal permittivity of BHK cells after infection are shown in Fig. 5 for both the interrupted and the continuous time course experiments. The graph represents the mean of the internal permittivities with the standard errors shown. Owing to the limitations in the data at high frequencies, the spread in the range of values is greater than for the specific capacitance. However, the trend in the data is clear and the average internal permittivity of cells taken from both the discontinuous and the continuous time course experiments are in good agreement with each other. It can be seen that the internal permittivity of BHK cells changes with time after infection. For uninfected cells the permittivity is $\epsilon_{int} = 75 \pm 12\epsilon_o$, which is in general agreement with other literature values obtained for mammalian cells (Huang et al., 1996). After infection with HSV-1 the internal permittivity drops by nearly $20\epsilon_o$ to a lower value of $\epsilon_{int} = 58 \pm 10\epsilon_o$ at 10 h after infection, thereafter remaining constant.

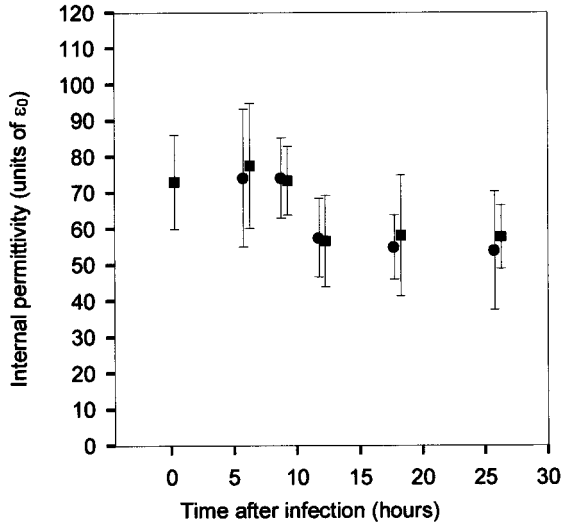

FIGURE 5 A plot of the time-dependent change in the internal permittivity of BHK(C-13) cells after infection with HSV-1. ●, continuous; ■, discontinuous time course experiments. For clarity, the points have been offset on the time axis by +0.25 h for the interrupted and −0.25 h for the continuous time course. Vertical bars show the standard error.

Internal conductivity

The time-dependent changes in the internal conductivity of BHK(C-13) cells after infection are shown in Fig. 6 for both the discontinuous and the continuous time courses. The graph represents the mean of the internal conductivities with the standard errors shown. The average value for the internal conductivity remains within the range 0.3–0.42 Sm^{-1} throughout the infectious cycle. This value can be compared with a growth medium conductivity of 1.4 Sm^{-1} and a suspending medium conductivity of 0.0175 Sm^{-1}.

DISCUSSION

Virus life cycle and cell ultrastructure

During infection of cells with HSV-1, the initial step is the binding of virions to cellular receptors, followed by fusion of the virion and cell membranes, leading to internalization of the virion components. In this work, the cells were infected with 10 pfu per cell of highly purified virus. With such a low number of virions binding to the cells, it is unlikely that they will have any directly measurable effect on the dielectric properties of a cell, particularly as it is a transient event. After membrane fusion, there is a rapid cascade of processes that result in a switch in gene expression from cellular to viral genes. However, the gross morphology of the cell was not detectably altered until several hours after infection when cells grown as monolayer cultures began to round up and lose their normal, extended conformation. This rounding proceeded until the cells were predominantly spherical by which stage they usually had detached from the tissue culture vessel. (In the experiments presented in this paper, all of the cells are spherical because they have been physically detached from the support for rotation measurements). The cause of the rounding appears to be the depolymerization of microtubules and of actin-containing microfilaments that are important for maintenance of the cellular ultrastructure. The cytoskeletal network is known to be important for transport of incoming viral DNA-containing capsids to the nucleus (Sodeik et al., 1997), but this is a very early event, which takes place before its disruption. It is not clear whether the disruption of the cytoskeleton is a functional feature of virus infection or simply a side effect of the drastic changes in macromolecular synthesis and organization that are consequent upon infection.

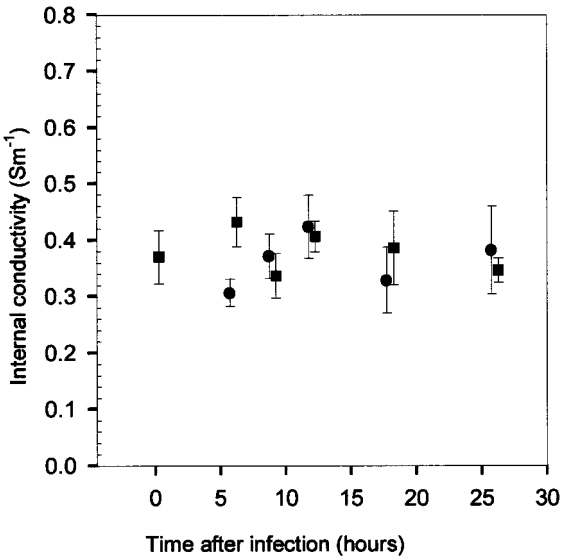

FIGURE 6 A plot of the time-dependent change in the internal conductivity of BHK(C-13) cells after infection with HSV-1. ●, continuous; ■, interrupted time courses. For clarity, the points have been offset on the time axis by +0.25 h for the interrupted and −0.25 h for the continuous time course. Vertical bars show the standard error.

Membrane capacitance

Changes also occur in the cell membrane as infection progresses, although the physical nature of these changes has not been well studied. Both increases (Krempein et al., 1984; Katsumoto et al., 1981) and decreases (Schlehofer et al., 1979b) in the numbers of microvilli have been reported after HSV infection of mammalian cells, as well as the formation of larger structures (folds and blebs). One consistent feature is the appearance of progeny virions on the cell surface. In BHK(C-13) cells, these start to appear ~6 h after infection, and their numbers increase markedly until approximately 12 h, after which they decline again (Rixon et al., 1992). The changes in the membrane ultrastructure are apparent in both the dielectric data and the SEM images (Fig. 4) of the cells. As these images show, there was an obvious change in the morphology of the membrane as infection progressed, but they do not indicate that there were any major changes in the shape of the cells. All of the cells were spherical owing to detachment from the culture vessel. However, there was a tendency toward more uniform rounding as infection progressed, as evidenced by a reduction in the size and number of irregular surface folds and creases, which was accompanied by an increase in the numbers of microvilli (Fig. 4).

It appears that the membrane of the detached uninfected cell has large-scale irregularities, including folds and creases, and that this changes to a more uniform conformation after infection, probably as a result the disruption of the cytoskeleton. This effect is apparent in the time dependency of the specific membrane capacitance where, between 6 and 9 h after infection, there was a rapid decrease of approximately 25%, compared with an uninfected cell. At this time exocytosis is well under way. The decrease in capacitance continues with time, both as the surface of the cell becomes smoother and the overall surface area reduces, together with the fact that the cell membrane takes on the composition of the viral envelope.

Membrane permeability and internal conductivity

Although the virus leaves the cell by exocytosis, this is not accompanied by cell lysis. The plasma membrane therefore retains its integrity throughout the productive phases of the infectious cycle. It is not known whether membrane permeability is affected, although decreases in membrane fragility after HSV infection have been reported for a number of mammalian cell types (Schlehofer et al., 1979a). To estimate the permeability of the cell membrane, dielectrophoretic crossover frequency measurements (Huang et al., 1996) were made on mock-infected cells and cells 18 h after infection. In both cases the membrane conductivity was too small to accurately measure using this method (<10 S/m^2), so that it can be concluded that the membrane does not become permeable during exocytosis.

Fig. 6 shows that the internal conductivity of the cell remained unchanged throughout the life cycle of the virus between 0.3 and 0.42 Sm^{-1} during the entire time course of the experiments for all the cells measured. This can be compared with the growth medium conductivity of 1.4 Sm^{-1}. This implies that the membrane did not become appreciably permeable as a result of virus exocytosis.

Internal permittivity

By 6 h after infection, virus particles are beginning to be made and the process of virus release begins. Virus capsids are synthesized in the nucleus and transported across the nuclear membrane. The capsids are surrounded by the tegument proteins and pass through the Golgi apparatus, where they probably acquire the viral envelope (Genderen et al., 1994; Browne et al., 1996), before exiting the cell. The fraction of the cytoplasmic volume occupied by membrane bound-vacuoles increases as a result of infection, as infection of cells with HSV-1 is known to cause proliferation of Golgi-derived membranes, generating large numbers of vacuoles (many containing virus particles) of different sizes (Smith and Harven, 1973). The synthesis of a large number of vacuoles and enveloped virions could lead to a marked reduction in the permittivity of the cytoplasm. The step change in internal permittivity occurred sometime between 9 and 12 h after infection, when large quantities of virions are being produced. This suggests that processes that give rise to large numbers of vacuoles are switched on at $\sim$9–12 h, and thereafter their rate of loss, by fusion with the plasma membrane, is probably equal to the rate of production. Thus, the reduction in internal permittivity could be attributed to an increase in the number of membrane-containing structures (vacuoles and virions) within the cell cytoplasm during viral replication.

Prospects

Dielectrophoresis can be used as a method for separating cells of different dielectric properties. For example, human breast cancer cells (MDA231) have been separated from normal human lymphocytes using a dielectrophoretic affinity column (Becker et al., 1995). The electrorotation spectrum for a particular cell type can be analyzed to give the frequency-dependent dielectric properties of the cells and thus develop optimal cell separation conditions or protocols. For the particular case of the BHK(C-13) cells, before and after infection, the corresponding dielectrophoretic spectrum was calculated from the electrorotation data, and the results are shown in Fig. 7. This figure shows the real and imaginary components of the factor $(\epsilon_p^* - \epsilon_{med}^*)/(\epsilon_p^* + 2\epsilon_{med}^*)$ (the Clausius-Mossotti factor), which gives an indication of the force and torque on a particle respectively, plotted for a medium conductivity of 17.5 mSm^{-1}. The curves are computed from the mean values of the dielectric parameter set, for mock-infected cells (curve *a*) and for cells 18 h after infection (curve *b*). The error bars represent the maximal deviation that occurs in the data, computed from the maximal standard error in the measured dielectric parameters for all the cells.

It can be seen from Fig. 7 that over a frequency window from 20–40 kHz, the uninfected cells experience a positive dielectrophoretic force whereas the cells 18 h after infection experience negative dielectrophoresis, implying that the two cell types could be successfully separated in an appropriate electrode chamber.

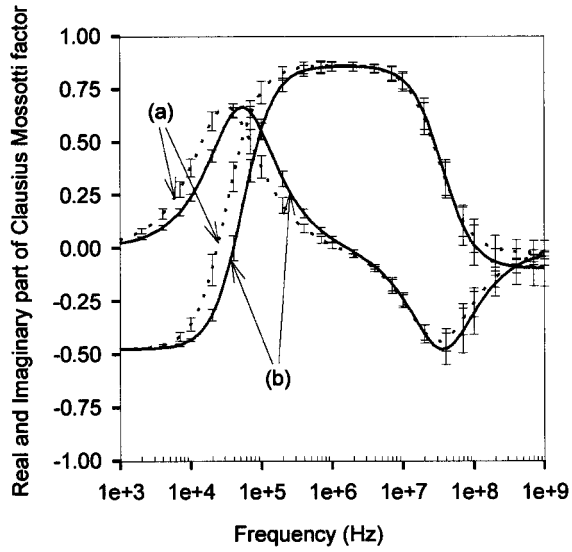

FIGURE 7 The frequency dependence of the real and imaginary components of the Clausius-Mossotti factor for BHK cells calculated from the electrorotation data (see text). Curve (*a*), dotted line is the Clausius-Mossotti factor for uninfected cells; curve (*b*), solid line, is the Clausius-Mossotti factor for cells infected for 18 h. Both curves are for a suspending medium conductivity of 17.5 mSm^{-1}. The error bars represent the limits in the data calculated from the range of the experimentally derived dielectric parameters. The plot shows that at this conductivity and in a frequency window from 20 to 40 kHz the two types of cells could be separated using dielectrophoretic methods.

CONCLUSIONS

We have shown that electrorotation can be used as a technique to probe the time-dependent biophysical changes that take place as a cell undergoes viral invasion, replication, and release. It has been shown that the membrane capacitance of the cells changes markedly between 6 and 9 h after infection, presumably as a result of changes in the morphology of the cell membrane. SEM images of cells, taken at discrete times after infection, indicate that the membrane morphology varied with the virus life cycle. There does not appear to be a measurable change in the conductivity of the membrane as a result of exocytosis, and the internal conductivity of the cell remains constant throughout the virus replication cycle at 0.3 to 0.42 Sm^{-1}, compared with the growth medium conductivity of 1.4 Sm^{-1}. A step change in internal permittivity was recorded at between 9 and 12 h after infection, which correlates with the increased generation of Golgi-apparatus-derived membranes that envelop the virions within the cytoplasm.

This work points to the potential application of electrorotation techniques as a method for the noninvasive analysis of virus-host interactions. Additional refinements to the technique, such as confinement of cells in electrical or optical traps, would allow single-cell measurements to be made and for data from a single cell to be collected over the entire 24-h life cycle of virus infectivity. The work also suggests additional biomedical applications and highlights the potential of dielectrophoretic separation techniques for the retrieval and separation of infected cells from uninfected cells.

We thank Mrs. Joyce Mitchell and Ms. Mary Robertson for virus preparation and Mr. Jim Aitken for preparation of samples for SEM.
This work was supported in part by the Biotechnology and Biological Sciences Research Council (UK) grant 17/T05315.

REFERENCES

Arnold, W. M., R. K. Schmutzler, S. Al-Hasani, D. Krebs, and U. Zimmermann. 1989. Differences in membrane properties between unfertilised and fertilised single rabbit oocytes demonstrated by electro-rotation: comparison with cells from early embryos. *Biochim. Biophys. Acta.* 979:142–146.

Arnold, W. M., and U. Zimmermann. 1988. Electro-rotation: development of a technique for dielectric measurements on individual cells and particles. *J. Electrostat.* 21:151–191.

Becker, F. F., X. B. Wang, Y. Huang, R. Pethig, J. Vykoukal, and P. R. C. Gascoyne. 1995. Separation of human breast cancer cells by differential dielectric affinity. *Proc. Natl. Acad. Sci. U.S.A.* 92:860–864.

Browne, H., S. Bell, T. Minson, and D. W. Wilson. 1996. An endoplasmic reticulum-retained herpes simplex virus glycoprotein H is absent from secreted virions: evidence for reenvelopement during egress. *J. Virol.* 70:4311–4316.

Fuhr, G., J. Gimsa, and R. Glaser. 1985a. Interpretation of electrorotation of protoplasts. I. Theoretical considerations. *Stud. Biophys.* 108: 149–164.

Fuhr, G., J. Gimsa, and R. Glaser. 1985b. Interpretation of Electrorotation of protoplasts. II. Interpretation of experiments. *Stud. Biophys.* 109: 5–14.

Gascoyne, P. R. C., F. F. Becker, and X. B. Wang. 1995. Numerical analysis of the influence of experimental conditions on the accuracy of dielectric parameters derived from electrorotational measurements. *Bioelectrochem. Bioenerg.* 36:115–125.

Gascoyne, P., R. Pethig, J. Satayavivad, F. F. Becker, and M. Ruchirwat. 1997. Dielectrophoretic detection of changes in erythrocyte membranes following malarial infection. *Biochim. Biophys. Acta.* 1323:240–252.

Genderen, I. L. V., R. Brandumarti, M. R. Torrisi, G. Campadelli, and G. V. Meer. 1994. The phospholipid composition of extracellular herpes simplex virions differ from that of the host cell nuclei. *Virology.* 200: 831–836.

Gimsa, J., P. Marszalek, U. Loewe, and T. Y. Tsong. 1991. Dielectrophoresis and electrorotation of neurospora slime and murine myeloma cells. *Biophys. J.* 60:749–760.

Gimsa, J., T. Muller, T. Schnelle, and G. Fuhr. 1996. Dielectric spectroscopy of single human erythrocytes at physiological ionic strength: dispersion of the cytoplasm. *Biophys. J.* 71:495–506.

Gimsa, J., C. Pritzen, and E. Donath. 1989. Characterisation of virus-red-cell interaction by electrorotation. *Stud. Biophys.* 130:123–131.

Gimsa, J., T. Schnelle, G. Zechel, and R. Glaser. 1994. Dielectric spectroscopy of human erythrocytes: investigations under the influence of nystatin. *Biophys. J.* 66:1244–1253.

Green, N. G. 1998. Dielectrophoresis of sub-micrometer particles. Ph.D. thesis. University of Glasgow, Glasgow.

Holzel, R. 1993. A simple wide-band sine wave quadrature oscillator. *IEEE Trans. Instrum. Meas.* 42:758–760.

Holzel, R. 1997. Electrorotation of single yeast cells at frequencies between 100 Hz and 1.6 GHz. *Biophys. J.* 73:1103–1109.

Hu, X., W. M. Arnold, and U. Zimmermann. 1990. Alterations in the electrical properties of T and B lymphocyte membrane induced by mitogenic stimulation: activation monitored by electro-rotation of single cells. *Biochim. Biophys. Acta.* 1021:191–200.

Huang, Y., R. Holzel, R. Pethig, and X. B. Wang. 1992. Differences in the AC electrodynamics of viable and non-viable yeast cells determined through combined dielectrophoresis and electrorotation studies. *Phys. Med. Biol.* 37:1499–1517.

Huang, Y., and R. Pethig. 1991. Electrode design for negative dielectrophoresis. *Meas. Sci. Technol.* 2:1142–1146.

Huang, Y., X. B. Wang, F. F. Becker, and P. R. C. Gascoyne. 1996. Membrane changes associated with the temperature-sensitive $P85^{gag\text{-}mos}$-dependent transformation of rat kidney cells as determined by dielectrophoresis and electrorotation. *Biochim. Biophys. Acta.* 1282: 76–84.

Huang, Y., X. B. Wang, R. Holzel, F. F. Becker, and P. R. C. Gascoyne. 1995. Electrorotational studies of the cytoplasmic dielectric properties of Friend murine erytholeukaemia cells. *Phys. Med. Biol.* 40:1789–1806.

Hughes, M. P., X. B. Wang, F. F. Becker, P. R. C. Gascoyne, and R. Pethig. 1994. Computer-aided analyses of electric fields used in electrorotation studies. *J. Phys. D Appl. Phys.* 27:1564–1570.

Hutchinson, L., C. Roop-Beaucamp, and D. C. Johnson. 1995. Herpes simplex virus glycoprotein K is known to influence fusion of infected cells, yet is not on the cell surface. *J. Virol.* 69:4556–4563.

Johnson, D. C., and P. G. Spear. 1982. Monensin inhibits the processing of herpes simplex virus glycoproteins, their transport to the cell surface, and the egress of virions from infected cells. *J. Virol.* 43:1102–1112.

Katsumoto, T., A. Hirano, T. Kurimura, and A. Takagi. 1981. In situ electron microscopical observations of cells infected with herpes simplex virus. *J. Gen. Virol.* 52:267–278.

Krempein, U., B. M. Jockisch, and C. Jungwirth. 1984. Herpes simplex virus-induced cell surface protrusions. *Intervirology.* 22:156–163.

Leslie, J., F. J. Rixon, and J. McLauchlan. 1996. Overexpression of Herpes Simplex Virus Type 1 tegument protein VP22 increases its incorporation into virus particles. *Virology.* 220:60–68.

Morgan, C., H. M. Rose, M. Holden, and E. Jones. 1959. Electron microscopic observations on the development of herpes simplex virus. *J. Exp. Med.* 110:643–656.

Pethig, R. 1991. Biological electrostatics: dielectrophoresis and electrorotation. *Inst. Phys. Conf. Ser.* 118:13–26.

Rixon, F. J., C. Addison, and J. McLauchlan. 1992. Assembly of enveloped tegument structures (L particles) can occur independently of virion

maturation in herpes simplex virus type 1-infected cells. *J. Gen. Virol.* 73:277–284.

Schlehofer, J. R., K.-O. Habermehl, W. Diefenthal, and H. Hampl. 1979a. Reduction of ^{51}Cr-permeability of tissue culture cells by infection with herpes simplex virus type 1. *Intervirology.* 11:158–166.

Schlehofer, J. R., H. Hampl, and K.-O. Habermehl. 1979b. Differences in the morphology of herpes simplex virus infected cells. I. Comparative scanning and transmission electron microscopic studies on HSV-1-infected HEp-2 and chick embryo fibroblast cells. *J. Gen. Virol.* 44: 133–442.

Smith, J. D., and E. D. Harven. 1973. Herpes simplex virus and human cytomegalovirus replication in WI-38 cells. I. Sequence of viral replication. *J. Virol.* 12:919–930.

Sodeik, B., M. W. Ebersold, and A. Helenius. 1997. Microtube-meditated transport of incoming herpes simplex virus 1 capsids to the nucleus. *J. Cell Biol.* 136:1007–1021.

Stephens, M., M. S. Talary, R. Pethig, A. K. Burnett, and K. I. Mills. 1996. The dielectrophoresis enrichment of CD34+ cells from peripheral blood stem cell harvests. *Bone Marrow Transplant.* 18:777–782.

Steven, A. C., and P. G. Spear. 1997. Herpesvirus capsid assembly and envelopment. *In* Structural Biology of Viruses. W. Chiu, R. M. Burnett, and R. L. Garcea, editors. Oxford University Press, Oxford. 312–351.

Szilagyi, J. F., and C. Cunningham. 1991. Identification and characterisation of a novel non-infectious herpes simplex virus-related particle. *J. Gen. Virol.* 72:661–668.

Wang, X. B., Y. Huang, P. R. C. Gascoyne, F. F. Becker, R. Holzel, and R. Pethig. 1994. Changes in Friend murine erythroleukaemia cell membranes during induced differentiation determined by electrorotation. *Biochim. Biophys. Acta.* 1193:330–344.

Wang, X. B., Y. Huang, R. Holzel, and J. P. H. Burt. 1993. Theoretical and experimental investigations of the interdependence of dielectric, dielectrophoretic and electrorotational behaviour of colloidal particles. *J. Phys. D Appl. Phys.* 26:312–322.

Wang, X. B., R. Pethig, and T. B. Jones. 1992. Relationship of dielectrophoretic and electrorotational behaviour exhibited by polarized particles. *J. Phys. D Appl. Phys.* 25:905–912.

Wang, J., V. L. Sukhorukov, C. S. Djuzenova, U. Zimmermann, T. Muller, and G. Fuhr. 1997. Electrorotational spectra of protoplasts generated from giant marine alga *Valonia utricularis. Protoplasma.* 196:123–134.

Wicher, D., J. Gundel, and H. Matthies. 1987. Electrorotation of liposomes in the α- and β-dispersion range. *Stud. Biophys.* 119:103–104.

Zhou, X. F., G. H. Markx, and R. Pethig. 1996. Effect of biocide concentration on electrorotation spectra of yeast cell. *Biochim. Biophys. Acta.* 1281:60–64.